Electron and nuclear dynamics of molecular clusters in ultraintense laser fields. I. Extreme multielectron ionization

Isidore Last and Joshua Jortner[a)]
School of Chemistry, Tel Aviv University, Ramat Aviv, 69978 Tel Aviv, Israel

(Received 22 November 2002; accepted 8 October 2003)

In this paper we present a theoretical and computational study of extreme multielectron ionization (involving the stripping of all the electrons from light, first-row atoms, and the production of heavily charged ions, e.g., Xe^{+q} $(q \leqslant 36)$ from heavy atoms) in elemental and molecular clusters of Xe_n, $(D_2)_n$, and $(CD_4)_n$ $(n=55-1061)$ in ultraintense (intensity $I=10^{15}-10^{19}\,W\,cm^{-2}$) laser fields. Single atom or molecule multielectron ionization can be adequately described by the semiclassical barrier suppression ionization (BSI) mechanism. Extreme cluster multielectron ionization is distinct from that of a single atomic or molecular species in terms of the mechanisms, the ionization level and the time scales for electron dynamics and for nuclear motion. The novel compound mechanism of cluster multielectron ionization, which applies when the cluster size (radius R_0) considerably exceeds the barrier distance for the BSI of a single constituent, involves a sequential-parallel, inner-outer ionization. The cluster inner ionization driven by the BSI for the constituents is induced by a composite field consisting of the laser field and inner fields. The energetics and dynamics of the system consisting of high energy ($\leqslant 3$ keV) electrons and of $\lesssim 100$ keV ions in the laser field was treated by molecular dynamics simulations, which incorporate electron–electron, electron–ion, ion–ion, and charge-laser interactions. High-energy electron dynamics also incorporates relativistic effects and includes magnetic field effects. We treat inner ionization considering inner field ignition, screening and fluctuation contributions as well as small [$(\leqslant 13\%)$] impact ionization contributions. Subsequent to inner ionization a charged nanoplasma is contained within the cluster, whose response to the composite (laser+inner) field results in outer ionization, which can be approximately described by an entire cluster barrier suppression ionization mechanism. © *2004 American Institute of Physics.* [DOI: 10.1063/1.1630307]

I. INTRODUCTION

Ultraintense table-top laser sources delivering ~1 J per pulse of duration of ~20–100 fs are characterized by the power of $\sim 10\,TW\,(10^{13}\,W)$ and by a maximal intensity of $\sim 10^{20}\,W\,cm^{-2}$, which constitutes the highest light intensity on earth,[1] providing new avenues in the exploration of light-matter interaction. The interaction of clusters with such ultrashort and ultraintense ($I=10^{15}-10^{20}\,W\,cm^{-2}$) laser fields triggers ultrafast dynamics of electrons (on a time scale of 1–100 fs, mostly 1–10 fs) and of ions (on a time scale of 10–100 fs).[2–24] The dynamics of electrons involves the inner ionization process, which strips the cluster atoms or molecules of some or of all of their electrons, and the outer ionization process, which removes all or part of the unbound electrons from the cluster.[15–18] The outer ionization is accompanied by Coulomb explosion,[16,19] which results in the production of energetic ions. Generally speaking, all three processes, i.e., inner ionization, outer ionization, and Coulomb explosion, are coupled to each other.[16] However, there is a hierarchy in the cause, time scales, and consequences of these processes. The cluster ionization process is initiated by the inner ionization, which provides the conditions for the outer ionization. The femtosecond and sub femtosecond time intervals of the inner and of the outer ionizations may overlap, but usually the inner ionization prevails on a shorter scale than the outer ionization.[16] We shall focus on electron dynamics and novel ionization mechanisms of molecular clusters in ultraintense laser fields ($I=10^{15}-10^{19}\,W\,cm^{-2}$), proceeding via a hierarchy of parallel-sequential, inner-outer ionization processes, while the facets of the nuclear dynamics of Coulomb explosion will be reported in the accompanying paper.[25]

In this paper, we study extreme multielectron ionization in representative elemental and molecular clusters, i.e., atomic clusters of xenon, Xe_n, and molecular clusters of deuterium $(D_2)_n$ and of deuterated methane $(CD_4)_n$ $(n=55-1061)$ in ultraintense ($I=10^{15}-10^{19}\,W\,cm^{-2}$) laser fields, using classical dynamics simulations. Extreme multielectron ionization involves the removal of the valence electrons or the complete stripping of all the electrons with the formation of nuclei in light, first-row atoms, or the formation of highly charged ions, e.g., Xe^{q+} $(q \leqslant 26)$, from heavy atoms. We shall address the ionization mechanisms and the ionization levels of multielectron cluster ionization in ultraintense laser fields, focusing on the novel and unique features of cluster ionization, which differ from those of the ionization of individual atoms and molecules.

II. MULTIELECTRON IONIZATION OF A SINGLE ATOM OR MOLECULE

In order to describe the process of cluster multielectron ionization one has to treat the electrons bound to the host

a)Electronic mail: jortner@chemsg1.ac.il

atoms (ions) and the unbound electrons. The bound electrons, whose motion is of strictly quantum character, are of interest only in the context of the inner ionization process. Atomic ionization in a strong electromagnetic field, whose frequency is considerably smaller than the ionization potential, can be considered as electron removal through an electrostatic barrier in a static electric field.[26] Due to tunneling effects the ionization probability depends, generally speaking, on the quantum parameters of the electron motion.[27–30] When the tunneling through such a barrier is of minor importance, a classical barrier suppression ionization (BSI) mechanism can be applied.[31]

The ionization of a single neutral atom or a k-fold charged atomic ion is triggered by the BSI when the potential U_b, at the top of the electrostatic barrier formed by the Coulomb field of the $(k+1)$ charge and the outer field, is equal, with opposite signs, to the ionization potential (IP), P_k, of this ion.[31] Then U_b is

$$U_b = -2[eFB(k+1)]^{1/2}, \tag{1}$$

where $B = 14.385\ \text{eV Å}$ and eF is the force (in eV Å^{-1}) exerted by the electric field **F** on the removed electron. The barrier is located at the distance

$$x_b = [B(k+1)/eF]^{1/2} \tag{2}$$

from the ion along the electric field **F** direction. For a single atomic or molecular species $F = F_\ell$, being the laser electric field, F_ℓ, while for a cluster (Sec. IV) F is the sum of the laser field and the inner cluster field. The laser field F_ℓ is related to the laser intensity I (expressed in W cm^{-2}) by

$$|eF_\ell| = 2.745 \times 10^{-7} I^{1/2}\ \text{eV Å}^{-1}. \tag{3}$$

Equating $|U_b|$, Eq. (1), and IP P_k one obtains the condition for the ionization of a neutral atom $(k=0)$ or a k-fold charged ion,[16,31] with the field strength being

$$|eF| \geqslant eF_{b'}, \tag{4}$$

where the threshold field for inducing (classical) ionization is

$$eF_b = P_k^2/4B(k+1). \tag{4a}$$

Substituting eF_b, Eq. (4a), into Eq. (2) we obtain the barrier location for the threshold field

$$x_b = 2B(k+1)/P_k. \tag{2a}$$

For atomic multielectron ionization of Xe the BSI relation, Eq. (4), together with the atomic P_k data[32,33] (Fig. 1), is applicable for all k values. The application of the atomic BSI mechanism, Eqs. (1), (2), and (4), to molecules, e.g., D_2 and CD_4, requires some further considerations and extensions. In molecules, unlike atoms, the ionization process may be affected by the electron delocalization and by the non-Coulomb character of the electron potentials. The ionization of molecules is affected by quasiresonance effects,[34–36] while for the ionization of large organic molecules, e.g., benzene or aromatics, electron delocalization prevails.[37] In what follows we consider molecules with localized electron bonds where the quasiresonance phenomena can be ignored. We restrict ourselves to ''small'' molecules, e.g., D_2 and CD_4, which for the molecular radius r_M is smaller than the barrier

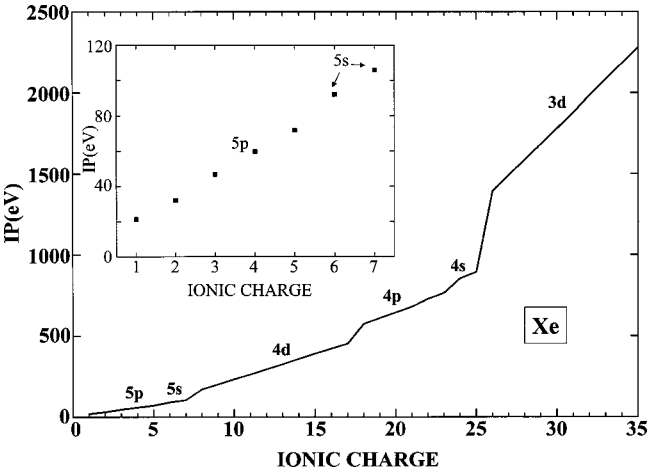

FIG. 1. Ionization potentials of Xe^{k+} ions. Data adopted from Refs. 32 and 33.

distances x_b (except for the inner C atom electrons). For $r_M < x_b$ an electron outside the molecule is subjected to a Coulomb potential and Eqs. (1), (2), and (4) can be used. The condition $r_M < x_b$ is expected to be very common for small molecules, as long as the outer shell atomic electrons are subjected to ionization. According to our estimates for diatomic molecules, the barrier distances x_b for the first ionization are mostly 2–3 times larger than the molecule radii r_M, which are defined as half of the interatomic distances. For the D_2 molecule considered in this work, at the equilibrium interatomic distance of 0.742 Å ($r_M = 0.37$ Å), the barrier distances, Eq. (2a), are considerably larger than r_M, i.e., $x_b = 1.86$ Å for the first ionization ($P_0 = 15.5\,\text{eV}$) and $x_b = 1.93$ Å for the second ionization ($P_1 = 29.8\,\text{eV}$).

Let us now consider the polyatomic methane molecule CD_4 whose radius is $r_M = R_{CD} = 1.09$ Å. The first ionization potential $P_0 = 12.9\,\text{eV}$ provides $x_b = 2.23$ Å, a value more than two times larger than r_M. The estimate of P_k for multielectron ionization for molecular ions $(CD_4)^{K+}$ $(k>0)$ becomes relatively simple for $K=5$ when the molecule is described as consisting of four deuterons D^+ and a carbon ion C^{k+} $(k=K-4)$. Applying a simple electrostatic model we express the ionization potential of such an ionic molecule as

$$P_K(C^{k+}D_4^+) = P_k(C^{k+}) + 4B/R_{CD}, \qquad K = 5-7, \quad k = 1-3. \tag{5}$$

The IPs of the $C^{k+}D_4^+$ $(k=1-3)$ molecular ion, estimated from Eq. (5), are presented in Table I. The barrier distances,

TABLE I. Ionization potentials, P_k, of atomic C^{k+} ions (see Ref. 32) and of C^{k+} ions in $C^{k+}D_4^+$ molecules. The IPs of molecular C^{k+} ions for $k=1-3$ are determined by Eq. (5) with $K=k+4$ standing for molecular charge. For $k=4-5$ the IPs of molecular C^{k+} ions coincide with IPs of atomic C^{k+} ions.

Electron state	$2p$	$2s$		$1s$	
k	1	2	3	4	5
K	5	6	7	4	5
$P_k(C^{k+})$ (eV)	24.4	47.9	64.5	392	490
$P_k(C^{k+}D_4^+)$ (eV)	77.2	101	117	392	490

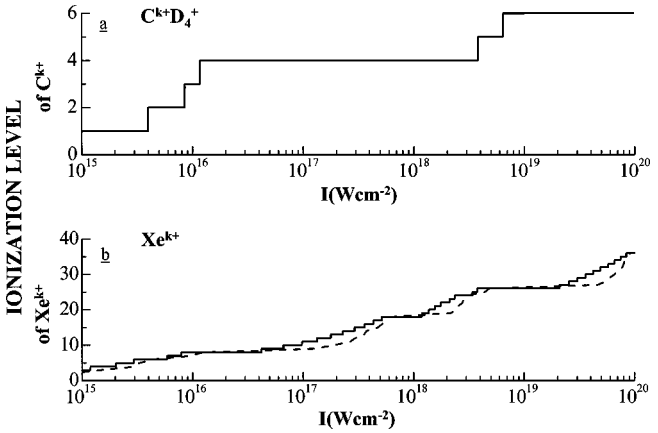

FIG. 2. The laser intensity (I) dependence of the ionization level of a single atom/molecule. Calculations (solid lines) within the framework of the barrier suppression ionization mechanism, Eq. (4a). (a) Carbon C^{k+} ion from the $C^{k+}D_4^+$ molecular ion. (b) Xenon Xe^{k+} ion. The dashed line represents the results of the ADK (see Ref. 27) approximation (see text).

Eq. (2), for the outer shell electrons of carbon ions are as follows: $x_b=1.86$, 1.71, 1.72 Å for $k=1$, 2, 3, respectively. These x_b values are larger than the molecule radius of $R_{CD}=1.09$ Å, which supports the use of the atomic relations, Eqs. (1), (2), and (4), for the $C^{k+}D_4^+$ ($k=1-3$) molecular ion. The barrier distances x_b for inner $(1s)^2$ electrons ($k=4-5$), which are also presented in Table I, are considerably smaller than R_{CD}, so that the removal of these electrons has to be considered as the ionization of the atomic C^{k+} ions.

The IPs of the Xe^{k+} ion for $k\leqslant 35$ (up to the ionization of $3d$ electrons)[32,33] are shown in Fig. 1. By substituting the IPs of the $C^{k+}D_4^+$ (Table I) and of the Xe^{k+} ions (Fig. 1) into Eq. (4a) we determined the dependence of the ionization level k of the $C^{k+}D_4^+$ and of the Xe^{k+} ions on the laser intensity I (Fig. 2). The ionization of all the valence electrons from $C^{k+}D_4^+$ is accomplished in the intensity domains $I=4\times10^{15}-2\times10^{16}$ W cm^{-2}, while stripping of all the electrons from CD_4 occurs at $I=6\times10^{18}$ W cm^{-2} [Fig. 2(a)]. The multielectron ionization of Xe is gradual with increasing I, reaching the ultrahigh ionic charge Xe^{36+} at $I=10^{20}$ W cm^{-2} [Fig. 2(b)].

The BSI model predictions for multielectron ionization of Xe atoms are in agreement with experiment. According to our BSI results for atomic xenon [Fig. 2(b)], the Xe^{8+} ion (with all the outer shell valence electrons being removed) is generated at $I>1.2\times10^{16}$ W cm^{-2}, which is larger by a numerical factor of 2 than the experimental threshold for the formation of these ions.[28] The experimental threshold for the formation of Xe^{20+} ions is $I\sim10^{18}$ W cm^{-2},[38] being close to the BSI prediction [Fig. 2(b)].

The calculated results for multielectron ionization of methane can only be qualitatively compared with experiments on organic molecules[8,39,40] in view of the differences in the inner fields and, in particular, differences in the effects of electron distribution in the methane molecule studied herein and in other organic molecules, which were experimentally studied.[38,39] According to our BSI results for the methane molecule [Fig. 2(a)] the C^{3+} and C^{4+} ions are generated at $I=8.5\times10^{15}$ and at $I>1.2\times10^{16}$ W cm^{-2}, respectively. The experimental study of Tzallas *et al.*[39] performed for the thiazole molecule provide a similar intensity of $I=6\times10^{15}$ W cm^{-2} for the generation of the C^{3+} ions. However, the experimental study of Lezius *et al.*[8] reports that the threshold for the formation of C^{3+} ions from some organic molecules is at a surprisingly low intensity of $\sim10^{14}$ W cm^{-2}. The threshold for the C^{4+} ion generation from C_{60} molecules was found to be $I=3\times10^{14}$ W cm^{-2},[40] which is more than an order of magnitude lower than the threshold intensity for C^{4+}, calculated herein for CD_4. Due to electron delocalization effects, the effective field in multielectron ionized C_{60} acting on C^{+k} ions may be larger as compared to that in $C^{k+}D_4^+$, resulting in enhanced ionization. Such ignition and electron delocalization effects on multielectron ionization will subsequently be discussed in Sec. VI for molecular clusters.

In order to check the validity of the classical BSI model we also performed the ionization probability calculations of Xe^{k+} ions using the quantum model of Amossov, Delone and Krainov (ADK).[27] The results of these calculations are presented in Fig. 2(b) as the $k(I)$ dependence (with the ionization level k being considered as a variable) for a fixed ionization probability of $w=1$ fs^{-1}. The ADK curve lies close to the $k(I)$ dependence obtained from the BSI mechanism, which confirms the validity of the classical BSI model on the time scale of $t\sim1$ fs. Similar results were also obtained for the ionization of the $1s$ electrons of carbon ions.

III. METHODOLOGY OF THE SIMULATIONS

When the laser wavelength is considerably longer than the cluster size, and the attenuation of light by the cluster is negligibly small, the laser field force acting on an electron is eF_ℓ, where the laser field is

$$F_\ell=F_{\ell0}(t)\cos(2\pi\nu t+\varphi_0). \tag{6}$$

The laser field force acting on a k-fold charged ion is $-keF_\ell$. The laser field frequency is taken as $\nu=0.35$ fs^{-1}, corresponding to the photon energy of 1.44 eV. We arbitrarily choose the initial phase as $\varphi_0=0$. Simulations were performed for a Gaussian-shaped pulse, which is characterized by the envelope

$$F_{\ell0}(t)=F_M\exp[-2.773(t/\tau)^2], \tag{7}$$

in the domain $t>-\infty$. The peak of the pulse is located at $t=0$, and τ is the width at the half maximum, $0.5F_M$. We take $\tau=25$ fs (the width of the half maximum of the intensity profile is 18 fs). The field maximum F_M is expressed by the peak laser intensity I in the laser focus volume, according to Eq. (3), with $F_\ell=F_M$ assuming that the attenuation of light in the focal volume is negligibly small.

For the Gaussian shaped laser pulse, Eq. (7), the process of inner ionization starts after the laser field F_ℓ becomes sufficiently strong to induce one-electron ionization of some constituent particles. We shall designate this ionization threshold field by F^{th}. In molecular clusters $(A_1A_2\ldots A_m)_n$ consisting of one kind of $A_1,A_2,\ldots,A_m$ molecules (where the indices 1,2...,m label the constituent atoms), F^{th} is equal to the threshold field F_b, Eq. (4a), with $k=0$, for the first ionization of each molecule and the production of

TABLE II. The first IP, P_0, and the mth (m being the number of atoms in a molecule) IP, P_{m-1} and the respective ionization fields F^{th} and F^{co}, Eq. (4a) for the Xe atom, and for the D_2 and the CD_4 molecules. $F_s=(F^{\text{th}}+F^{\text{co}})/2$. eF data are given in eV Å^{-1}. Representative laser peak fields are $eF_M=27.4$ eV Å^{-1} at $I=10^{16}$ W cm^{-2} and $I=274$ eV Å^{-1} at $I=10^{18}$ W cm^{-2}.

Molec.	Xe	D_2	CD_4
m	1	2	5
P_0	12.1	15.5	12.9
P_{m-1}	12.1	29.8	66.4
eF^{th}	2.54	4.18	2.89
eF^{co}	2.54	7.72	15.3
eF_s	2.54	5.95	9.10

$(A_1A_2\ldots A_m)^+$ molecular ions. We note that, in general, only partial one-electron ionization of the molecular cluster constituents is accomplished at F^{th}. A complete one-electron ionization of all the constituent atoms is achieved at a somewhat higher laser field, F^{co}. In $(A_1A_2\ldots A_m)_n$ clusters the F^{co} field is realized when each $A_1A_2\ldots A_m$ molecule of the cluster becomes a $A_1^+A_2^+\ldots A_m^+$ molecular ion. We determine F^{co} for the single molecular ionization by substituting the molecular IP, P_K for $K=m-1$ into Eq. (4a). The IP $(m=2)$ for D_2 was taken as the IP of the H_2^+ ionic molecule at the interatomic distance of the neutral H_2 molecule.[41] In the case of CD_4, the IP P_{m-1} for the production of the $C^+D_4^+$ ion from $C^+D_3^+D$ $(m=5)$ was found adopting the electrostatic approach, from P_K of Eq. (5), in the form

$$P_4(C^+D_3^+D)=P_0(D)+B/R_{CD}+3B/R_{DD}. \tag{8}$$

In the case of an elemental atomic cluster, e.g., Xe_n, $eF^{\text{co}}=eF^{\text{th}}$. The eF^{th} and eF^{co} values for $(D_2)_n$, $(CD_4)_n$, and Xe_n clusters are presented in Table II.

The two field strengths for the inner ionization of F^{th} and F^{co} distinguish three domains of different cluster ionization levels. In the first domain, $F<F^{\text{th}}$, all cluster particles are neutral. In the second domain, $F^{\text{th}}\leqslant F\leqslant F^{\text{co}}$, the $(A_1A_2\ldots A_m)_n$ cluster consists of partly ionized molecules $(A_1A_2\ldots A_m)^{k+}$, $k<m$, and unbound electrons. The interactions in such a cluster are very complicated due to the presence of dispersion and polarization interactions and due to the quantum effects of inter- and intramolecular positive charge delocalization.[42,43] In the third domain, $F_\ell>F^{\text{co}}$, the cluster consists of atomic ions and unbound electrons. In this domain the interparticle interactions are dominated by Coulomb forces, which simplify the simulation treatment.

Neglecting the overlap between atomic ions we present the ion–ion interaction by a Coulomb repulsion potential

$$U_{i-i}=Bk_1k_2/r_{12}, \tag{9}$$

where k_1 and k_2 stand for k_1 and k_2 fold ionized ions. The electron–ion interactions were represented by a Coulomb attraction potential modified by a smoothing term[16]

$$U_{e-i}=-Bk(r^6+r_0^6)^{-1/6}, \tag{10}$$

where k stands for a k-fold ionized ion. The values of the smoothing term are taken as $r_0=0.3$, 0.6, 1.0 Å for D^+, C^{k+}, and Xe^{k+} ions, respectively. The electron–electron potential is presented with a smoothing quadratic term[16]

$$U_{e-e}=B(r^2+\overline{r}_0^2)^{-1/2}, \tag{11}$$

with $\overline{r}_0=0.2$ Å. The smoothing parameters r_0 and $\overline{r}_0$ in Eqs. (10) and (11) were chosen as the corresponding minimal values which do not violate energy conservation. This approximate description of the electron–ion and electron–electron potentials underestimates small impact parameter collisions. Numerical tests of the insensitivity of the electron and ion energetics to changes of the smoothing parameter (within a numerical factor of 2) indicate that such small impact parameter collisions are not important.

Simulations using the potentials given by Eqs. (9)–(11) are valid only in the third domain of the inner ionization, i.e., for $F_\ell>F^{\text{co}}$. However, if we start the simulations at $F_\ell=F^{\text{co}}$ we ignore the ionization process which took place in the domain $F^{\text{th}}\leqslant F_\ell\leqslant F^{\text{co}}$. On the other hand, if we start the simulation at $F_\ell=F^{\text{th}}$, we overestimate the ionization level by asserting that all constituent atoms are ionized at the threshold field F^{th}.

The onset of the laser pulse, Eqs. (6) and (7), is in principle located at $t=-\infty$. In our simulations we used an initially truncated Gaussian pulse with the laser field F_s at a finite (negative) time $t=t_s$. In order to explore the effects of the rise time and initial field of the truncated pulse on the cluster dynamics, we performed simulations of the effect of the initial laser field F_s on the energetics $E(F_s)$ of the ions in the Coulomb explosion of multicharged $(D_2)_n$, $(CD_4)_n$, and $(Xe)_n$ clusters in laser fields corresponding to $I=10^{16}-10^{18}$ W cm^{-2} (Fig. 3). At the starting point of the simulation all cluster atoms are taken as singly charged ions, and the clusters are represented as $(D_2^+)_n$, $(C^+D_4^+)_n$, and Xe_n^+ with the geometry of neutral clusters, while the electrons are initially located at $r=x_b$ from the center of each singly ionized ion in the cluster. The onset fields eF^{th} and eF^{co} are given in Table II. To assess the effects of initial pulse truncation on the ion energies from Coulomb exploding clusters, we defined a reference initial field strength F_s^0 at large values of $|t_s|$, being $F_s^0<F^{\text{th}}$, with the initial ionization levels specified earlier. We performed simulations for the reference ion energies $E(F_s^0)$ and for the ion energies $E(F_s)$ at the different initial fields F_s and F_s^0, respectively (where $F_s>F_s^0$). Figure 3 displays the simulation results for the energy ratios $E(F_s)/E(F_s^0)$ versus F_s/F_M, where F_M is the peak field strength, Eq. (7). For the intensity range $I=10^{16}-10^{18}$ W cm^{-2} rather small effects are manifested for initial pulse truncation on the deuteron energetics from Coulomb explosion of molecular clusters, i.e., D^+ from $(D_2)_n$ and from $(CD_4)_n$ (Fig. 3). Changing the F_s/F_M ratio in the large range of 0–0.5, the effect of laser pulse truncation at $I=10^{18}$ W cm^{-2} increases the D^+ ion energies from $(D_2)_n$ by less than 8% and the D^+ ion energies from $(CD_4)_n$ by less than 18% [Fig. 3(a)]. At $I=10^{16}$ W cm^{-2}, the pulse truncation in the range $F_s/F_M=0-0.5$ increases the D^+ ion energies from $(D_2)_n$ by less than 4% [Fig. 3(b)], while the energies of D^+ from $(CD_4)_n$ decrease by about 12% [Fig. 3(b)]. The difference between the effects of pulse truncation on D^+ energies from $(CD_4)_n$ at the intensities $I=10^{16}$ and $I=10^{18}$ [Figs. 3(a) and 3(b)] originates from a delicate balance between cluster electron and nuclear dynamics. The

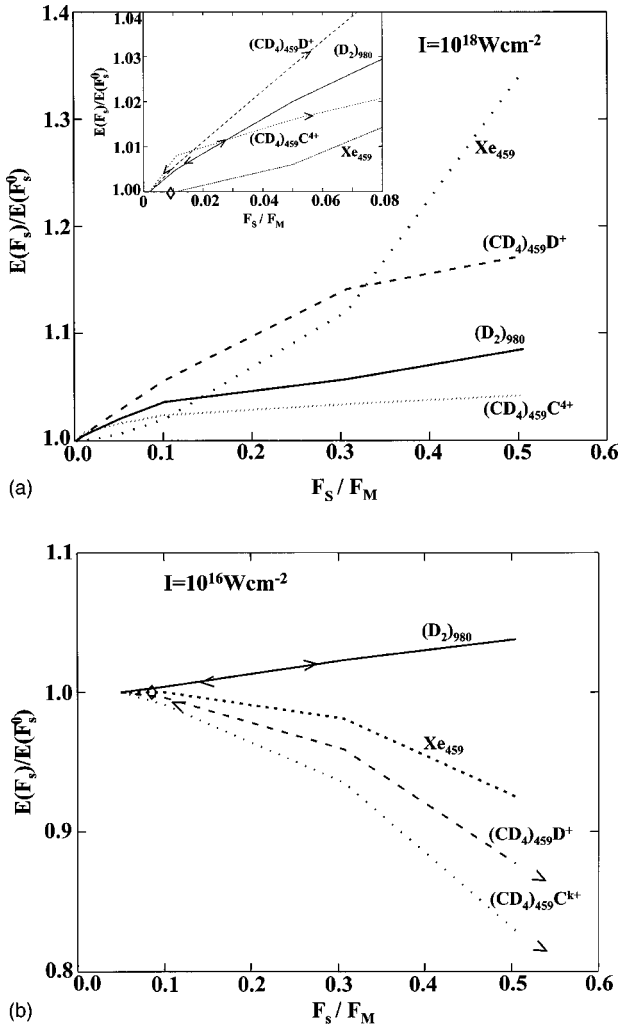

FIG. 3. The effect of initial laser pulse truncation at the laser field F_s on the energetics of D^+, C^{+k}, and Xe^{k+} ions from the Coulomb explosion of $(D_2)_n$ and from $(CD_4)_n$, C^{k+} $(k=3-4)$ from $(CD_4)_n$, and Xe^{k+} from Xe_n. The ion energies ratios are given by $E(F^{th})/E(F_s^0)$, and correspond to the ion energies $E(F_s)$ relative to the energies at the $E(F_s^0)$ low reference field F_s^0 below the threshold field F^{th} for the first ionization of each cluster molecule. The truncation field is given in terms of F_s/F_M where F_M is the laser peak field intensity. $<$ mark the values of F^{th}, and $>$ mark the values of F^{co}, which are different for $(D_2)_n$ and $(CD_4)_n$ clusters. When $F^{th}=F^{co}$ for Xe_n clusters, the value is marked by $\langle\,\rangle$. The labels on the curves correspond to the ions: Xe^{k+} $[Xe_{459}]$, D^+ $[(D_2)_n]$, D^+ $[(CD_4)_{459}D^+]$, C^{k+} $[(CD_4)C^{k+}]$. (a) $I=10^{18}\,W\,cm^{-2}$; (b) $I=10^{16}\,W\,cm^{-2}$.

rather small effects of laser field truncation on the energetics of D^+ ions imply the validity of our previously reported conclusions, based on simulations[20,21,23] of the energetics of deuterons from Coulomb explosion of $(D_2)_n$ and $(CD_4)_n$ clusters (where we took $F_s/F_M=0.5$).[16]

Regarding the energetics of heavy ions from molecular $(CD_4)_n$ clusters, the effect of changing F_s/F_M in the large range 0–0.5 results in the increase of the C^{4+} energy by less than 3% at $I=10^{18}\,W\,cm^{-2}$ and in the decrease of the energies of the C^{k+} ions $(k\simeq 3-4)$ by 17% at $I=10^{16}\,W\,cm^{-2}$ [Figs. 3(a) and 3(b)]. For elemental $(Xe)_n$ clusters the effects of pulse truncation are considerably larger at $I=10^{18}\,W\,cm^{-1}$, whereas in the range $F_s/F_M=0-0.5$ the energies of the Xe^{k+} $(k\simeq 18-24)$ ions increase by 35%, while at $I=10^{16}\,W\,cm^{-2}$ the energies of the Xe^{k+} ions $(k\simeq 4-11)$ decrease by 7% [Figs. 3(a) and 3(b)]. The change in the effects of laser truncation on the energetics of the heavy ions, i.e., C^{k+} from $(CD_4)_n$ and Xe^{k+} from Xe_n at different laser peak intensities, reflects again, as in the case of the D^+ ions, the interplay between electron and nuclear dynamics. In addition, as revealed by our simulations for $(Xe)_n$ clusters (which will not be presented here), the effect of pulse truncation is considerably larger due to the enhancement of the inner ionization level with the truncated pulses. From these simulations we conclude that, in the relevant laser ultrahigh intensity domain used herein, the effects of the pulse truncation on the energetics of D^+ and of light multicharged ions from the Coulomb explosion of molecular clusters are rather small (i.e., $<20\%$), and truncated pulses can be applied for simulations of cluster Coulomb explosion driving nuclear fusion,[20,23,44] which results in considerable saving of computer CPU time for the simulations.

Finally, we have to provide recipes for the choice of the parameters F_s and t_s for the pulse truncation to be used in the present simulations. From the foregoing specification of the values of F^{th} and F^{co} (marked in Fig. 3), we note that the energies of the product ions exhibit a weak dependence on F_s in the range $F_s<F_s^{co}$, so that $F^{th}\leqslant F_s\leqslant F^{co}$ will be adequate. In the present simulations we choose $F_s=(F^{th}+F^{co})/2$ (Table II).

The cluster inner ionization is driven by a composite field $\mathbf{F}=\mathbf{F}_\ell+\mathbf{F}_i$ consisting of laser field $\mathbf{F}_\ell$, Eq. (6), and inner fields $\mathbf{F}_i$, generated by the electrostatic interactions, Eqs. (9)–(11). BSI in the composite field $\mathbf{F}$ acts on each cluster constituent and differs qualitatively from single species ionization due to the inner field effects. When the condition of Eq. (4) is fulfilled, the cluster inner ionization event is initiated by locating the removed electron at point x_b, [Eq. (2a)], with zero kinetic energy. The multielectron ionization is realized in a sequential way, i.e., one electron being removed at each inner-ionization time step (20 attoseconds in our simulations). Such a ''static field'' ionization approximation was justified by the insensitivity of the simulation results for electron and ion dynamics to a time lag of <50 attoseconds, which is considerably lower than the reciprocal laser frequency (2.85 fs) used in the simulations. The unbound electrons, whose kinetic energy inside the cluster in a strong laser field falls in the range 35 eV ($\lambda\simeq 2$ Å)–20 keV ($\lambda\simeq 0.1$ Å), are treated by the classical mechanics approach. Since zero-point energy effects for the vibrations of heavy particles are of minor importance for the process of Coulomb explosion, the heavy particles are also considered as classical particles. Accordingly, the simulation of cluster ionization and Coulomb explosion processes with appropriate ultra short, i.e., attosecond, time intervals for the electron and nuclear dynamics is substantiated within the framework of the classical mechanics. Considering the electrons we take into account the electric field eF_ℓ acting on each electron, and also the forces generated by the magnetic component of the laser field.[16] Inside a cluster, according to our simulation results, the electron velocity is mostly small as compared to the light velocity, i.e., $v\ll c$, so that the contribution of the magnetic component of the laser field is not significant. However, outside a cluster the velocity of electrons is considerably higher

and the ratio v/c reaches the values of ~ 0.25 and ~ 0.75 at high laser intensities of 10^{18} and $10^{19}\,\mathrm{W\,cm^{-2}}$, respectively. At these intensities the magnetic field can significantly affect the electron motion, and the relativistic effects may be of importance, at least at $I \geqslant 10^{19}\,\mathrm{W\,cm^{-2}}$. To take these effects into account, the electron motion was treated by the relativistic approach, with scaling of the masses by $m = m_e[1-(v/c)^2]^{-1/2}$, and using classical mechanics for the electron dynamics in the simulations.

The numerical integration of the classical equations of motion of unbound electrons and of ions was performed with the time steps of 1 as and of 20–40 as, respectively. Simulations of the inner ionization, i.e., of the ionization of the atoms or molecules in the cluster, were based on the BSI mechanism (Sec. II). The removal of an unbound electron from a cluster, i.e., the outer ionization event, is recorded when the distance of this electron from the cluster center is more than six times larger than the cluster radius of the Coulomb expanding cluster. After the event of outer ionization is recorded, the electron is discarded from the simulation procedure. Since the electron–ion interactions are included explicitly in our simulations, the hydrodynamic pressure on ions associated with the high-energy electrons[3,5] is partially taken into account.

IV. CLUSTER INNER AND OUTER IONIZATION

The dependence of the ionization level k on the laser intensity I, presented in Fig. 2, is valid for single isolated $C^{k+}D_4^+$ and Xe^{k+} ions, where the ionization is determined by a single-step barrier suppression mechanism. Cluster multielectron intense-field ionization is distinct from that of a single atom or molecule. The mechanistic differences pertain to the novel sequential-parallel, inner-outer cluster ionization mechanism, which differs from that of a single species unistep ionization. For the onset of this compound cluster ionization mechanism the lower limit of the cluster size sets in when the cluster size R significantly exceeds the (single-species) barrier distance x_b, Eq. (2a), i.e., $R \gg x_b$, and the BSI mechanism for each cluster constituent produces an electron within the cluster. Under these circumstances one has to distinguish between inner and outer ionization processes, both of which are affected by the inner fields of the charged cluster.

The new features of cluster multielectron ionization are that:

(1) Due to inner field effects, the cluster inner ionization, which is driven by the composite field $\mathbf{F}_i + \mathbf{F}_\ell$ (Sec. III), differs qualitatively from single species ionization.
(2) The subsequent formation of a nonequilibrium plasma within the cluster (Fig. 4) constitutes a novel phenomenon and is not encountered for single-species ionization.
(3) The response of the plasma to the composite (laser +inner) field results in outer ionization.

The inner field effects, manifested during both inner and outer ionization, involve screening effects (which decrease the effective field), and ignition effects[45] (which increase the effective field). Any ion in the cluster is subjected not only to the laser (exterior) field, F_ℓ, but also to the inner field, F_i, generated by other ions and by the unbound electrons. In addition, at the onset of cluster ionization, when the laser field is small, the inner field is locally enhanced by charge fluctuations. One of the effects caused by the inner field is the ignition mechanism, which enhances the inner ionization.[45] This mechanism takes place in a cluster, which becomes positively charged due to the outer ionization process. If the number of the unbound electrons inside the cluster is small, then the inner field force $\mathbf{F}_i$ is oriented toward the center. At any time, depending on the direction of the field, about half of the cluster ions are subjected to the composite field $\mathbf{F}_\ell + \mathbf{F}_i$, which is larger than the laser field $\mathbf{F}_\ell$, contributing to the enhancement of the inner ionization level. The inner field $\mathbf{F}_i$ increases with increasing the distance from the center, resulting in the maximal effect for the peripheral ions. The effect of the inner field differs from that of the ignition mechanism when the number of unbound electrons inside a cluster is large. The motion of the highly mobile

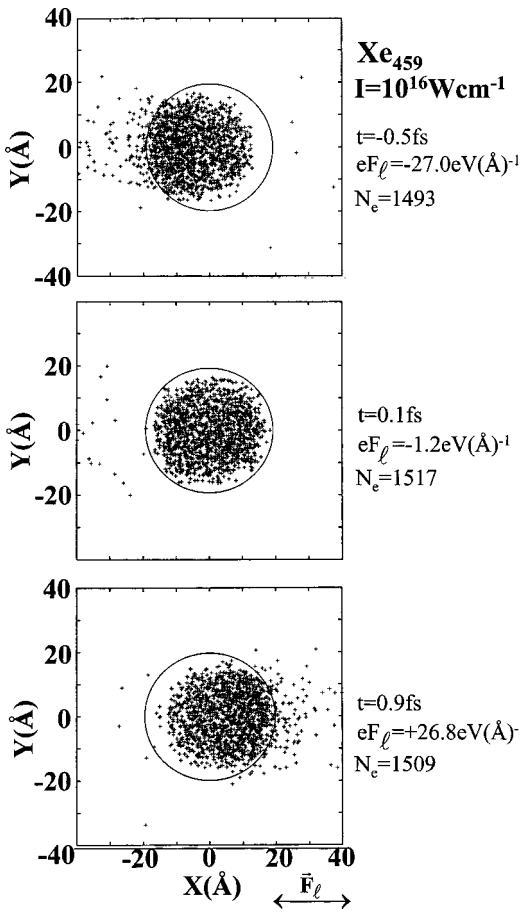

FIG. 4. The dynamics of the electron cloud (represented in two dimensions) in a Xe_{459} cluster at laser intensity $I = 10^{16}\,\mathrm{W\,cm^{-2}}$ and electric field direction along the x axis, as obtained from molecular dynamics simulations. The numbers represent the time t (in fs) and the laser field eF_ℓ (in eV Å^{-1}). The circles represent the cluster size. The laser fields eF_ℓ and the number of electrons N_e in the nanoplasma at each time are marked on each map. The maps show the oscillation of the nonequilibrium nanoplasma in the laser field, exhibiting left-side/right-side biased distribution when $eF_\ell = -27$ eV Å^{-1}/26.8 eV Å^{-1} and a nearly central distribution at a low value of $eF_\ell = 1.2$ eV Å^{-1}.

unbound electrons is roughly in a phase with the laser field (Fig. 4), providing a screening effect, which weakens the laser field and attenuates the inner ionization level. The screening effect is expected to be maximal in the inner region of the cluster. When the outer ionization process is highly effective, so that the unbound electrons are depleted from the cluster on a time scale close to that of their formation, the screening effect is expected to be weak and only the ignition mechanism can significantly affect the inner ionization. When the outer ionization is a less effective process and a large number of electrons is located inside a cluster for a relatively long time, the effects of both the ignition mechanism and the screening may be significant. Characteristic time scales for inner and outer ionization, which are determined by the time difference between the saturation and the threshold of the corresponding electronic processes, are 20–30 fs for $(CD_4)_{1061}$ at $I=10^{16}\,\mathrm{W\,cm^{-2}}$, and 10–13 fs for this cluster at $I=10^{18}\,\mathrm{W\,cm^{-2}}$,[25] manifesting laser intensity and pulse shape effects, cluster size dependence, and the dependence on the nature of constituents, which will be discussed in a subsequent paper.[25]

The inner field $\mathbf{F}_i$ is expected to manifest temporal fluctuations, due to electron density fluctuations in the nonequilibrium plasma. These inner field fluctuations may increase the composite field $\mathbf{F}_\ell+\mathbf{F}_i$ acting on some atoms and contributing to the increase of the atom ionization level. Taking into account the electron density fluctuations on neighboring atoms, which are located at the distances $R\sim 3-4$ Å, and assuming the charge density fluctuations to involve a few electrons, we estimate the inner field oscillation to be of the order of $eF_i\approx Bq/R^2\sim 1-4\,\mathrm{eV\,Å^{-1}}$. The effect of such a small field is of some importance only at the onset of the ionization process, when the low laser field is of the same order of magnitude as F_i and the ionization level of the atoms is still low. The fluctuation effects may enhance the inner ionization process at a low ionization level of the constituents, but most probably it does not affect the final ionization levels, which are determined by the laser field as well as by ignition and screening effects. The ignition mechanism, the screening effect, and the effect of plasma fluctuations are taken into account in our simulations.

In parallel with the barrier suppression mechanism the electron impact ionization can also contribute to the inner ionization.[16] The impact ionization events are determined here by using Lotz's model for the ionization of isolated atoms and ions.[46] This model was extended by us[16] for the electron impact ionization of atoms and ions in clusters and is utilized to estimate the contribution of impact ionization.

The inner ionization process results in an unequilibrated plasma (Fig. 4) in the cluster.[25] The removal of electrons from the plasma induced by the laser field constitutes the outer ionization process. The mechanisms of the outer ionization involve both the static laser field effects, i.e., BSI for the entire cluster (advanced in Sec. VI), as well as the dynamic quasiresonance effects.[14,16] These general considerations regarding mechanisms and time scales for cluster multielectron inner/outer ionization will now be confronted with the results of our simulations.

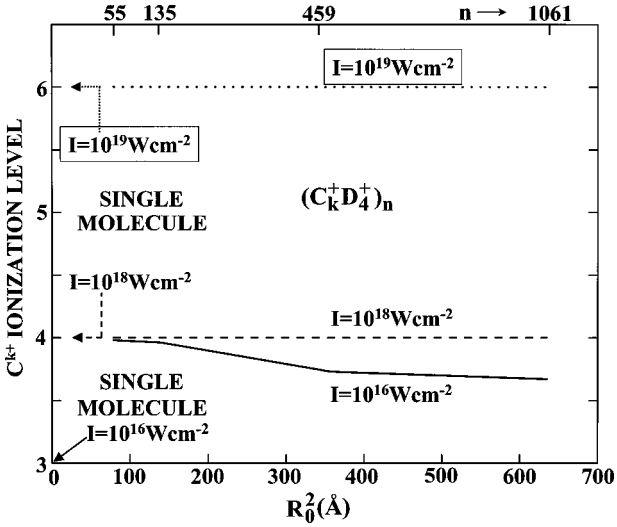

FIG. 5. Inner ionization of $(CD_4)_n$ clusters. The cluster size and laser intensity dependence of the average inner ionization level of C^{k+} ions for $(C^{k+}D_4^+)_n$ $(n=55-1061)$ clusters. The intensities are marked on the curves. The decrease of the ionization level with increasing n (and R_0^2) at $I=10^{16}\,\mathrm{W\,cm^{-2}}$ is due to the increase of screening effects. The difference between the (nearly saturated) ionization levels at the two highest intensities is due to the formation of C^{4+} at $I=10^{18}\,\mathrm{W\,cm^{-2}}$ and of C^{6+} at $I=10^{19}\,\mathrm{W\,cm^{-2}}$. The single molecule ionization levels at these intensities are marked by arrows.

V. CLUSTER INNER IONIZATION LEVEL

The simulations of cluster ionization were performed for methane deuterated clusters $(CD_4)_n$ at three laser intensities, i.e., $I=10^{16}$, 10^{18}, and $10^{19}\,\mathrm{W\,cm^{-2}}$, and for xenon clusters Xe_n at two laser intensities, i.e., $I=10^{16}$ and $10^{18}\,\mathrm{W\,cm^{-2}}$, while a restricted number of simulations were also performed for Xe_n at $I=10^{17}\,\mathrm{W\,cm^{-2}}$. Let us first consider the simulation results for the methane clusters.

In the $(CD_4)_n$ clusters at $I=10^{18}\,\mathrm{W\,cm^{-2}}$ all the C atoms become C^{4+} ions, i.e., they loose all the valence electrons but not the inner $(1s)^2$ electrons (Fig. 5). At $I=10^{19}\,\mathrm{W\,cm^{-2}}$ the C-ions loose all their electrons and become C^{6+} nuclei (Fig. 5). At these high laser intensities of 10^{18} and $10^{19}\,\mathrm{W\,cm^{-2}}$ the ionization level of the C ions inferred from our simulations is in accord with the BSI mechanism for a single molecule [Fig. 2(a)]. This implies that neither the ignition mechanism nor the screening effect contribute to the ionization level at this exceedingly high intensity. The situation is different at a lower laser intensity of $I=10^{16}\,\mathrm{W\,cm^{-2}}$ (Fig. 5). At this intensity the BSI model for a single molecule provides C^{3+} ions [Fig. 2(a)]. The simulation for the cluster results in the average ionization level of C atoms, which is slightly lower than $k=4$ and decreases slowly with increasing the cluster size. The distribution of the C^{k+} ionic charges is nonuniform and spatially inhomogeneous. For example, the C^{k+} ion charges from the $(CD_4)_{1061}$ cluster are distributed over a wide interval of $1\leqslant k\leqslant 4$, with a relative abundance of 0.2%, 6.2%, 17.5%, and 76.1% for $k=1$, 2, 3, and 4, respectively. The weakly charged ions with $k<3$ are located in the inner region of the clusters, whereas the C^{4+} ions are located mainly at the cluster periphery. The presence of a large number of

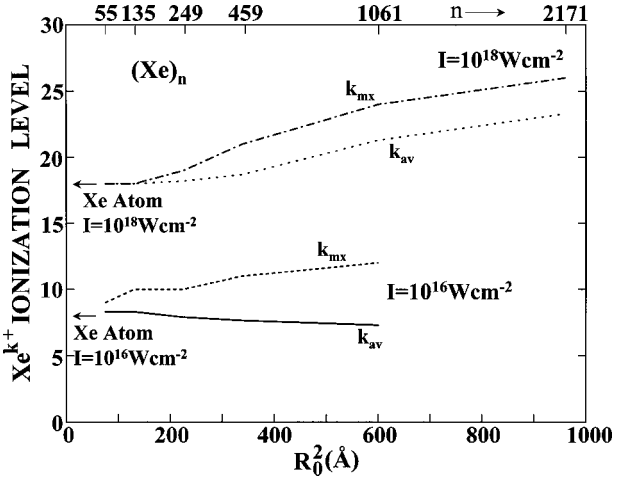

FIG. 6. The cluster size and the laser intensity dependence of the average (k_{av}) and maximal (k_{mx}) inner ionization level of Xe^{k+} ions (left scale) for $(Xe)_n$ clusters ($n=55-1061$). At the intensity of $I=10^{16}\,W\,cm^{-2}$, the decrease of k_{av} with increasing I is due to screening effects. Intensities are marked on the curves. At the high intensity of $I=10^{18}\,W\,cm^{-2}$ the increase of the inner ionization levels k_{mx} and k_{av} with increasing the cluster size is due to inner field (ignition) effects. The ionization levels of a single Xe atom at these intensities are marked by arrows.

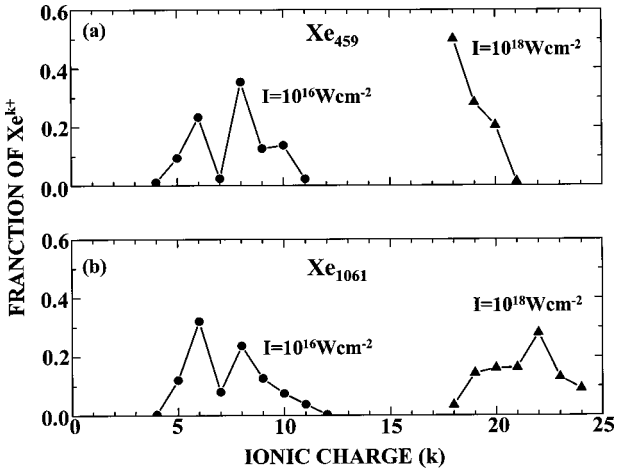

FIG. 7. The charge distribution of Xe^{k+} ions in the Coulomb explosion products of $(Xe)_{459}$ [panel (a)] and $(Xe)_{1061}$ [panel (b)] clusters at $I=10^{16}\,W\,cm^{-2}$ and at $I=10^{18}\,W\,cm^{-2}$. Cluster sizes are marked on the panels and intensities are marked on the curves.

C^{4+}, C^{+}, and C^{2+} ions and their location in the cluster indicates that the inner ionization in these clusters is affected by both the ignition mechanism (at the cluster periphery) and by the screening effect (in the inner cluster region). In the $(CD_4)_n$ clusters C^{4+} ions represent the saturation limit of the ionization level up to the intensity of $I=10^{18}\,W\,cm^{-2}$. At higher intensities of $I\geqslant 10^{19}\,W\,cm^{-2}$, C^{6+} carbon nuclei manifest the saturation level.

In the Xe_n clusters, in contrast to the $(CD_4)_n$ clusters, there is no saturation limit for the increase of the Xe-ion ionization level by increasing the laser intensity I, at least not in the domain of $I\leqslant 10^{19}\,W\,cm^{-2}$ considered herein [Fig. 2(b)]. With increasing the ionization level the jumps in the IP values, which manifest the ionization of other electron shells, are also not as large as in the case of carbon ions (Fig. 1 and Table I). Consequently, we have a wider interval of the ionic charges and a stronger dependence of the average ionization level k_{av} on the laser intensity. The laser intensity of $I=10^{16}\,W\,cm^{-2}$ generates the Xe^{8+} atomic ions [Fig. 2(b)] for a single atom, according to the BSI mechanism. In all the Xe_n clusters studied herein the average ionization level k_{av} is somewhat lower than $k=8$ for this laser intensity, decreasing with increasing the cluster size (Fig. 6). The maximal ionization level k_{mx} is, however, larger than $k=8$ (some ions lose a few $4d$ electrons by the BSI mechanism) and also increases with increasing the cluster size (Fig. 6). As discussed earlier, the less charged ions are concentrated in the central region of the clusters whereas the higher charged ions are located at the cluster periphery. These features of inner ionization at $I=10^{16}\,W\,cm^{-2}$ (Fig. 6) strongly indicate the manifestation of both the screening effect and the ignition mechanism. At the larger laser intensity of $I=10^{18}\,W\,cm^{-2}$ the BSI mechanism for single atoms provides Xe^{18+} ions with the outer electronic shell of $(4s)^2(4p)^6$ [Fig. 2(b)]. In the small Xe_{55} and Xe_{135} clusters the average k_{av} and the maximal k_{mx} ionization levels are equal to $k=18$, coinciding with the single atom ionization levels (Fig. 6). For Xe_n, $n\geqslant 249$, both these k values increase with increasing the cluster size, due to the ignition mechanism, reaching $k_{av}=22.3$ and $k_{mx}=26$ [outer shell configuration $(3d)^{10}$] for Xe_{1061}.

The ionization level distribution of the Xe^{k+} ions produced by Coulomb explosion are shown in Fig. 7 for Xe_{459} and Xe_{1061} clusters at $I=10^{16}\,W\,cm^{-2}$ and at $I=10^{17}\,W\,cm^{-2}$. At $I=10^{16}\,W\,cm^{-2}$ the distributions are nearly cluster size independent, and are similar, with two maxima, at $k=6$ and $k=8$, and with a minimum at $k=7$. At $I=10^{18}\,W\,cm^{-2}$ the minimal ionization level is $k=18$ (all the $5p$, $5s$, and $4d$ electrons being removed) for both clusters. However, the shape of the distributions is different. For the smaller Xe_{459} cluster, the fraction of ions decreases monotonously with increasing k, whereas for the larger Xe_{1061} cluster the distribution demonstrates a maximum at $k=22$. The maximal ionization level for the Xe_{1061} cluster is $k_{mx}=24$ (with the removal of all $4p$ electrons), as compared to $k_{mx}=21$ for Xe_{459}. The differences between the ionization level distribution for Xe_{459} and Xe_{1061} at $I=10^{18}\,W\,cm^{-2}$ is due to the ignition mechanism, which is strong at the high intensity and whose effect increases with the cluster size.

In addition to the BSI, electron impact ionization in the cluster provides an additional contribution to the inner ionization process. The number of impact ionization events is relatively small. The fraction of impact ionization events at $I=10^{18}\,W\,cm^{-2}$ was found to be less than 1% for Xe_n clusters and less than 6% for $(CD_4)_n$, $n\leqslant 1061$, clusters. At lower intensities of $I=10^{16}\,W\,cm^{-2}$ the fraction of impact ionization events is larger, reaching 13% and 9.5% for $(CD_4)_{1061}$ and Xe_{1061} clusters, respectively (Fig. 8). The fraction of impact ionization events increases with the cluster size, being roughly proportional to the square of the initial cluster radius R_0^2. In order to estimate the effect of the impact ionization on the inner ionization level, we performed simulations which ignore the impact ionization mechanism. It was found that ignoring the impact ionization only slightly decreases the average ionization level k_{av} [e.g., for $(CD_4)_{459}$ at

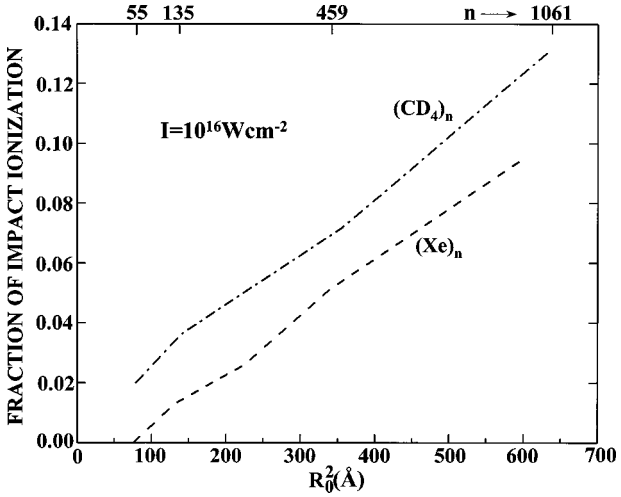

FIG. 8. The cluster size dependence of the relative impact ionization yield for $(CD_4)_n$ and Xe_n ($n=55-1061$) clusters. The fraction of impact ionization is expressed relatively to the inner ionization due to the BSI mechanism. The (small) relative impact ionization yield increases linearly with increasing R_0^2.

$I=10^{16}\,\mathrm{W\,cm^{-2}}$ $k_{\mathrm{av}}=3.79$ and 3.58 with and without impact ionization, respectively] and does not at all change the maximal ionization level k_{mx}. The effect of the input ionization on the ion energy is minor, being of the order of 0.1%–0.4%.

The experimental studies performed by Ditmire *et al.*[3,5] at $I=2\times10^{16}\,\mathrm{W\,cm^{-2}}$ reported very high ionization levels of the Xe atoms, up to $k_{\mathrm{mx}}=35-45$, in the Xe_{2500} ($R_0\approx32$ Å) clusters. Even for a considerably higher intensity of $I=10^{18}\,\mathrm{W\,cm^{-2}}$ our simulations provide a lower ionization level of $k_{\mathrm{mx}}=24$ for Xe_{1061}. At the smaller laser intensity of $I=10^{16}\,\mathrm{W\,cm^{-2}}$, our simulations provide $k_{\mathrm{mx}}=12$ for the same cluster (Figs. 6 and 7). There is a possibility that impact ionization may induce the high ionization level in the $(Xe)_{2500}$ clusters experimentally studied.[3,5] One may argue that the energy of electrons, according to the experiments[5] and to our simulations,[16] is sufficiently large (up to 3000 eV) to produce Xe^{40+} ions. However, using our scaling rule of $\sim R_0^2$ for impact ionization, we were unable to obtain a significant increase of the ionization levels for the Xe_{2500} cluster as compared to those studied herein for the Xe_{1061} cluster. The discrepancy between the experimental data[3,5] and our simulation results may at least be partly explained by the inhomogeneity of the laser focus volume. The clusters subjected to a higher intensity than the average intensity of $I=2\times10^{16}\,\mathrm{W\,cm^{-2}}$,[3,5] can produce ions with a higher charge. In the work of Lezius *et al.*,[47] Xe^{25+} and Xe^{30+} ions were detected in very large clusters, $n\sim2\times10^6$, subjected to a strong laser intensity of $I=5\times10^{17}\,\mathrm{W\,cm^{-2}}$. These experimental results are consistent with our simulation results, which provide maximum charged ions Xe^{24+} for much smaller, $n=1061$, clusters subjected to a laser intensity of $I=10^{18}\,\mathrm{W\,cm^{-2}}$ (Figs. 6 and 7).

Our simulation results reveal the important difference between the features of the inner ionization of the first-row atoms, like C, and of much heavier atoms, like Xe in the *n* corresponding clusters. In a wide interval of laser intensities [$10^{16}\,\mathrm{W\,cm^{-2}}<I<3\times10^{18}\,\mathrm{W\,cm^{-2}}$ for a single C atom, Fig. 2(a)] the first-row Z-number single atoms A lose their outer shell electrons and become $A^{(Z-2)+}$ ions, in accordance with Eq. (4a). At a very high intensity [$I>7\times10^{18}\,\mathrm{W\,cm^{-2}}$ for a single C atom, Fig. 2(a)] they also lose the inner electrons and become A^{Z+} nuclei. In contrast, the much heavier atoms are expected to increase the ionization level almost smoothly with the increasing laser intensity, and for the laser intensities available at present they cannot be deprived from all their electrons, whereupon the formation of heavy nuclei by multielectron ionization is precluded.

VI. CLUSTER OUTER IONIZATION

The outer ionization process removes all, or part, of the unbound electrons, which were formed by inner ionization, from the cluster by the laser field. We will describe this process by an electrostatic model, similar to the barrier suppression model of a single atom (or single molecule) ionization (see Sec. II), which will be applied to the cluster as a whole. This cluster barrier suppression ionization (CBSI) model involves the balancing between the cluster exterior Coulomb potential and the laser field potential at the cluster boundary.

The most favorable depletion region for the removal of unbound electrons from the cluster is located in the vicinity of the cluster's border on the diameter directed along the laser effective field. Electrons with a low kinetic energy will be removed from the depletion region to infinity, provided that the force exerted by the laser electric field exceeds BQ/R^2, with R and Q being the cluster radius and total charge, respectively. Taking into account the oscillatory character of the laser field we replace the electrostatic effective field by the mean square root $F_\ell/\sqrt{2}$ of the amplitude F_ℓ of the laser envelope function, Eq. (7), whereupon the balancing condition at the cluster boundary is

$$eF_\ell/\sqrt{2}\geqslant BQ/R^2. \tag{12}$$

Let us consider the temporal domain with rising of the laser field [$t<0$ in Eq. (7)], when the saturation of the inner ionization process is realized, with a fixed cluster ionic charge being Q_I, while the number of unbound electrons n_e inside the cluster decreases due to the outer ionization process. The total cluster charge is then $Q=Q_I-n_e$, increasing with time. We assume that, in the course of the outer ionization process, the redistribution of electrons inside the cluster is fast on the time scale for the process so that there are always some unbound electrons in the favorable depletion region referred to earlier. Equation (12) then provides the condition for the occurrence of outer ionization (at time t), with n_e unbound electrons remaining in the cluster

$$eF_\ell=\sqrt{2}B(Q_I-n_e)/R^2. \tag{13}$$

Equation (13) characterizes the dynamics of outer ionization, expressed in terms of the number of interior unbound electrons $n_e(t)$ for a given value of the laser field amplitude $F_\ell(t)$, Eq. (7), for a fixed laser peak $F_\ell(t)<F_M$, where F_M corresponds to the peak intensity. Concurrently, the nuclear dynamics of the cluster Coulomb explosion, which is ex-

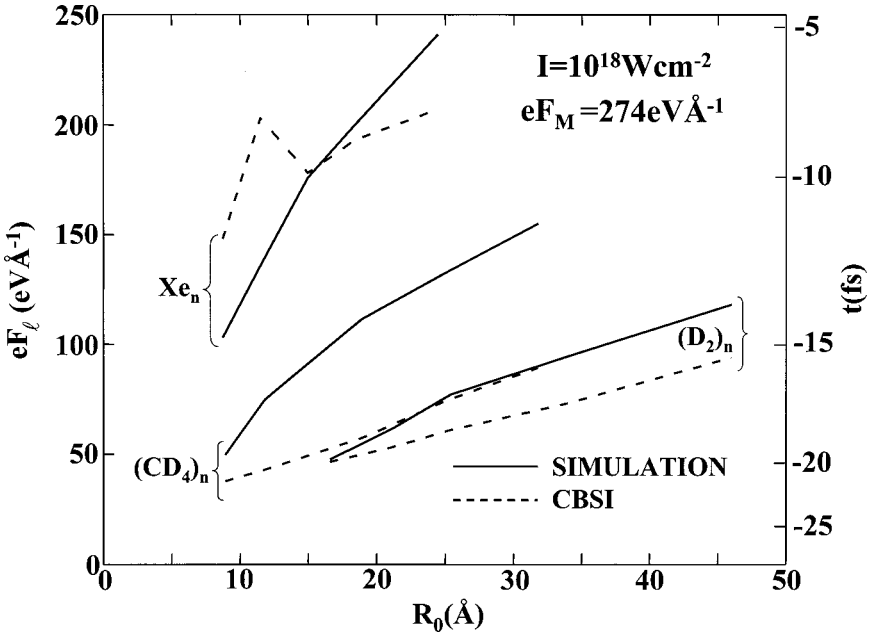

FIG. 9. The cluster size dependence of the minimal laser field strength eF_ℓ required for the removal of all the unbound nanoplasma electrons from $(D_2)_n$, $(CD_4)_n$, and Xe_n clusters (note that $eF_\ell < eF_M$). The simulation data (solid line) are compared with the results of the CBSI model, Eq. (15) (dashed line). The right scale represents the time scale for the attainment of the laser field eF_ℓ according to Eqs. (6) and (7).

pressed in terms of the time dependent cluster radius, $R(t)$, is known from the simulations. At the onset of the outer ionization process $R(t)=R_0$. Substituting $n_e=0$ into Eq. (13), we can estimate the minimal laser field $(eF_\ell)_{ino}$, which induces the complete removal $(n_e=0)$ of all the unbound electrons from the cluster as

$$(eF_\ell)_{ino}=\sqrt{2}BQ_I/R^2, \tag{14}$$

which can be expressed in the form

$$(eF_\ell)_{ino}=(4\pi\sqrt{2}/3)B\rho_{\mathrm{mol}}q_{\mathrm{mol}}R_0\xi^2, \tag{15}$$

where R_0 is the initial cluster radius, ρ_{mol} is the initial molecular density (in Å^{-3}), q_{mol} is the final molecular charge, and $\xi=R_0/R$ is a correction factor for the expansion of the cluster radius due to Coulomb explosion. Equation (15) constitutes the CBSI model for outer ionization, providing an effective, approximate cluster size equation for the outer ionization process.

In order to check the validity of the CBSI model, we compared in Fig. 9 the simulation results obtained for $(eF_\ell)_{ino}$ for $(D_2)_n$, $(CD_4)_n$ and $(Xe)_n$ clusters at $I=10^{18}\,\mathrm{W\,cm^{-2}}$ $(eF_M=274\,\mathrm{eV\,Å^{-1}})$ with the results evaluated from the CBSI model, Eq. (15), using molecular density and charge data, together with the correction factor ξ (<1), obtained for all clusters from the simulations of the cluster radius. The use of Eq. (15) requires the data for the densities ρ_{mol} and molecular charges q_{mol}. For $(D_2)_n$ $\rho=0.025\,\text{Å}^{-3}$ and $q_{\mathrm{mol}}=2$, while for $(CD_4)_n$ $\rho=0.016\,\text{Å}^{-3}$ and $q_{\mathrm{mol}}=8$. In the case of $(Xe)_n$ $(\rho=0.017\,\text{Å}^{-3})$ the q_{mol} values (in the relevant range) were also obtained from the simulation. The "critical" fields eF_ℓ for complete outer ionization (Fig. 9) calculated from Eq. (15) reveal an overall increase of eF_ℓ with increasing the initial cluster radius for (D_2), $(CD_4)_n$, and Xe_n clusters in accord with the simulation results (Fig. 9). The only exception from the monotonous increase of eF_ℓ with increasing R_0 is the behavior of eF_ℓ vs R_0 for $(Xe)_n$ clusters, which manifests an (unexplained) irregular cluster size dependence according to Eq. (15), which is not observed in the simulation results. The CBSI analysis of outer ionization for $(D_2)_n$ clusters is in good agreement with the simulation results (Fig. 9). On the other hand, for $(CD_4)_n$ clusters deviations between the CBSI estimates and the simulation results are more pronounced. The overall agreement between the $(eF_\ell)_{ino}$ values from the CBSI model, Eq. (15), and the simulation results for $(CD_4)_n$ clusters is within a numerical factor of $\lesssim 2$. This relatively large deviation is due to the occurrence of two distinct effective cluster radii, i.e., those for D^+ and those for C^{4+} ions in the Coulomb explosion expansion. From this analysis we conclude that the CBSI model provides a reasonable, semiquantitative description of the cluster outer ionization.

VII. CONCLUDING REMARKS

Extreme cluster multielectron ionization in an ultraintense laser field $(I=10^{14}-10^{19}\,\mathrm{W\,cm^{-2}})$ is a rich research area, being distinct from that of a single-species (i.e., atom or molecule) ionization, in terms of mechanisms, nature of ionic products and time scales for electron and nuclear dynamics. The ultraintense field for single-species ionization is dominated by the semiclassical barrier suppression mechanism (the BSI mechanism), where quantum effects are eroded. The BSI provides a clear distinction between the laser intensity I dependence of the ionization level of light, first-row atoms, e.g., H, D, and T or C, and heavy atoms, e.g., Xe. The light H, D, and T atoms are deprived from their only electron at $I>4\times10^{13}\,\mathrm{W\,cm^{-2}}$, while C^{k+} ions saturate with the formation of the bare nucleus $(k=6)$ at high $(I=10^{19}\,\mathrm{W\,cm^{-2}})$ intensities. On the other hand, for heavy atom ionization, e.g., Xe^{k+}, high-order multielectron atomic ionization is manifested by a gradual increase of the ionization level with increasing I (Sec. III).

When the cluster size R (or the size of a large scale chemical system) significantly exceeds the size of the constituent barrier distance x_b, Eq. (2a), i.e., $x_b \ll R$, a compound cluster ionization mechanism is manifested, which occurs via a sequential-simultaneous, inner-outer ionization process. The cluster inner ionization is qualitatively similar, but quantitatively different from that of a single-species ionization. The cluster inner ionization produces a nanoplasma within the cluster and in its vicinity, which retards further charge separation. The inner field effects within the multicharged clusters result in plasma screening effects, which decrease the effective field, and in an ignition ionization mechanism, which increases the effective field for the inner ionization process. The screening effect and the ignition mechanism are local, being determined by the location of the ion in the cluster. Our molecular dynamics simulations incorporate both the screening effects and the ignition mechanism. The ionization level of the cluster atoms is determined by the inner ionization process (which includes the inner field effects), with electron–ion recombination effects being negligible.[16] In addition to the BSI induced by laser and inner field effects in the cluster, an additional low-yield ionization process in the cluster prevails via electron impact ionization. The electron impact ionization yield empirically scales as $\propto R_0^2$, and decreases with increasing I, i.e., for Xe_{1061} the yield is $\sim 9\%$ at $I=10^{16}\,\mathrm{W\,cm^{-2}}$ and $\sim 1\%$ at $I=10^{18}\,\mathrm{W\,cm^{-2}}$. The effect of the impact ionization on the ions energy is very weak, being less than 0.4%. Ultraintense laser fields induce extreme multielectron ionization. Our simulations predict the formation of Xe^{26+} ions from multielectron ionization of Xe_{2171} clusters at $I=10^{18}\,\mathrm{W\,cm^{-2}}$, in accord with the experimental data of Lezius *et al.*[47] On the other hand, our prediction ($k_{\mathrm{mx}}=12$) for $I=10^{16}\,\mathrm{W\,cm^{-2}}$ (Fig. 6) underestimates the ionization level ($k=35-40$) of Xe_n ($n=1000-2000$) clusters reported by Ditmire *et al.*,[5] a discrepancy which may be due to the spatial inhomogeneity of the laser intensity in those experiments. Finally, the laser intensity dependence of the cluster multielectron ionization yield manifests a saturation of the ionization yield with the formation of bare light nuclei at very high intensities [i.e., C^{6+} formation from $(CD_4)_n$ at $I=10^{19}\,\mathrm{W\,cm^{-2}}$] and a smooth increase of the ionization level with increasing I in heavy atom clusters (e.g., Xe_n) precluding the formation of heavy nuclei.

Subsequent to the formation of the nonequilibrium nanoplasma in the cluster, the outer ionization process sets in. The cluster outer ionization mechanism is unique for the large finite system, and does not prevail for the single species ionization. The cluster outer ionization constitutes a complicated process of intracluster plasma ionization by the laser field. A heuristic and oversimplified description of outer ionization involves the CBSI mechanism (Sec. VI), with the electrostatic barrier being located at the cluster boundary. In this simple picture the energy transfer from the laser field to the unbound electrons within the cluster is transcendented by a quasiresonance mechanism, which is manifested by the oscillations of the center of mass of the unbound electron cloud along the light polarization direction and will be addressed in the accompanying paper.[25]

ACKNOWLEDGMENT

This research was supported by the James Franck Binational German-Israeli Program in Laser-Matter Interaction.

[1] G. A. Mourou, C. P. J. Barty, and M. D. Perry, Phys. Today **51**, 22 (1998).
[2] E. M. Snyder, S. Wei, J. Purnell, S. A. Buzza, and A. W. Castleman, Jr., Chem. Phys. Lett. **248**, 1 (1996).
[3] T. Ditmire, J. W. G. Tisch, E. Springate, M. B. Mason, N. Hay, R. A. Smith, J. Marangos, and M. H. R. Hutchinson, Nature (London) **386**, 54 (1997).
[4] K. Kondo, A. B. Borisov, C. Jordan, A. McPherson, W. A. Schroeder, K. Boyer, and C. K. Rhodes, J. Phys. B **30**, 2707 (1997).
[5] T. Ditmire, E. Springate, J. W. G. Tisch, Y. L. Shao, M. B. Mason, N. Hay, J. P. Marangos, and M. H. R. Hutchinson, Phys. Rev. A **55**, 369 (1998).
[6] J. V. Ford, O. Zhong, L. Poth, and A. W. Castleman, Jr., J. Chem. Phys. **110**, 6257 (1999).
[7] L. Köller, M. Schumacher, J. Köhn, J. Tiggesbäumker, and K. H. Meiwes-Broer, Phys. Rev. Lett. **82**, 3783 (1999).
[8] M. Lezius, V. Blanchet, D. M. Rayner, D. M. Villeneuve, A. Stolov, and M. Yu. Ivanov, Phys. Rev. Lett. **86**, 51 (2001).
[9] E. Springate, N. Hay, J. W. G. Tisch, M. B. Mason, T. Ditmire, M. H. R. Hutchinson, and J. P. Marangos, Phys. Rev. A **61**, 063201 (2000).
[10] J. Zweiback, R. A. Smith, T. E. Cowan, G. Hays, K. B. Wharton, V. P. Yanovsky, and T. Ditmire, Phys. Rev. Lett. **84**, 2634 (2000).
[11] J. Zweiback, T. E. Cowan, R. A. Smith *et al.*, Phys. Rev. Lett. **85**, 3640 (2000).
[12] S. Teuber, T. Töppner, T. Fennel, J. Tiggesbäumker, and K. H. Meiwes-Broer, Eur. Phys. J. D **16**, 59 (2001).
[13] V. Kumarappan, M. Krishnamurthy, D. Mathur, and L. C. Tribedy, Phys. Rev. A **63**, 023203 (2001).
[14] D. A. Card, E. S. Wisniewski, D. E. Folmer, and A. W. Castleman, Jr., J. Chem. Phys. **116**, 3554 (2002).
[15] T. Ditmire, Phys. Rev. A **57**, R4094 (1998).
[16] I. Last and J. Jortner, Phys. Rev. A **62**, 013201 (2000).
[17] K. Ishikava and T. Blenski, Phys. Rev. A **62**, 063204 (2000).
[18] V. P. Krainov and A. S. Roshchupkin, Phys. Rev. A **64**, 063204 (2001).
[19] I. Last and J. Jortner, Phys. Rev. A **60**, 2215 (1999).
[20] I. Last and J. Jortner, Phys. Rev. A **64**, 063201 (2001).
[21] I. Last and J. Jortner, Phys. Rev. Lett. **87**, 033401 (2001).
[22] P. B. Parks, T. E. Cowan, R. B. Stephens, and E. M. Campbell, Phys. Rev. A **63**, 063203 (2001).
[23] I. Last and J. Jortner, J. Phys. Chem. A **106**, 10877 (2002).
[24] G. Grillon, Ph. Balcou, J.-P. Chambaret *et al.*, Phys. Rev. Lett. **89**, 065005 (2002).
[25] I. Last and J. Jortner, J. Chem. Phys. **120**, 1348 (2004), following paper.
[26] L. V. Keldysh, Sov. Phys. JETP **20**, 1307 (1965).
[27] M. V. Amossov, N. B. Delone, and V. P. Krainov, Sov. Phys. JETP **64**, 1191 (1986).
[28] G. Gibson, T. S. Luk, and C. K. Rhodes, Phys. Rev. A **41**, 5049 (1990).
[29] A. Becker, L. Plaja, P. Moreno, M. Nurhuda, and F. H. M. Faisal, Phys. Rev. A **64**, 023408 (2001).
[30] D. Fisher, Y. Maron, and L. P. Pitaevskii, Phys. Rev. A **58**, 2214 (1998).
[31] S. Augst, D. Strickland, D. D. Meyerhofer, S. L. Chin, and J. Eberly, Phys. Rev. Lett. **63**, 2212 (1989).
[32] R. D. Cowan, *The Theory of Atomic Structure and Spectra* (University of California Press, Berkeley, 1981).
[33] Th. A. Carlson, C. W. Nestor, Jr., N. Wasserman, and J. D. McDowell, At. Data **2**, 63 (1970).
[34] T. Zuo and A. D. Bandrauk, Phys. Rev. A **52**, R2511 (1995).
[35] T. Seideman, M. Yu. Ivanov, and P. B. Corkum, Phys. Rev. Lett. **75**, 2819 (1995).
[36] I. Last and J. Jortner, Phys. Rev. A **58**, 3826 (1998).
[37] J. Jortner, S. Leutwyler, and Z. Berkovitch-Yellin, J. Chem. Phys. **78**, 309 (1983).
[38] M. Dammasch, M. Dörr, U. Eichmann, E. Lenz, and W. Sandner, Phys. Rev. A **64**, 061402R (2001).
[39] P. Tzallas *et al.*, Chem. Phys. Lett. **343**, 91 (2001).
[40] R. C. Constantinescu *et al.*, Phys. Rev. A **58**, 4637 (1998).
[41] D. R. Bates, K. Lenstram, and A. L. Stewart, Philos. Trans. R. Soc. London, Ser. A **246**, 215 (1953).

[42] F. X. Gadea and M. Amarouche, Chem. Phys. **140**, 385 (1990).
[43] I. Last and Th. George, J. Chem. Phys. **93**, 8925 (1990).
[44] J. Jortner and I. Last, ChemPhysChem **3**, 845 (2002).
[45] C. Rose-Petruck, K. J. Schafer, K. R. Wilson, and C. P. J. Barty, Phys. Rev. A **55**, 1182 (1997).
[46] W. Lotz, Z. Phys. **216**, 241 (1968).
[47] M. Lezius, S. Dobosh, D. Normand, and M. Schmidt, Phys. Rev. Lett. **80**, 261 (1998).